Neuroendocrine androgen action is a key extraovarian mediator in the development of polycystic ovary syndrome

Aimee S. L. Caldwell[a], Melissa C. Edwards[a,b], Reena Desai[a], Mark Jimenez[a], Robert B. Gilchrist[b], David J. Handelsman[a], and Kirsty A. Walters[a,b,1]

[a]Andrology Laboratory, ANZAC Research Institute, University of Sydney, Sydney, NSW 2139, Australia; and [b]Discipline of Obstetrics and Gynaecology, School of Women's and Children's Health, University of New South Wales, Sydney, NSW 2052, Australia

Edited by Bruce S. McEwen, The Rockefeller University, New York, NY, and approved February 23, 2017 (received for review October 5, 2016)

Polycystic ovary syndrome (PCOS) is a complex hormonal disorder characterized by reproductive, endocrine, and metabolic abnormalities. As the origins of PCOS remain unknown, mechanism-based treatments are not feasible and current management relies on treatment of symptoms. Hyperandrogenism is the most consistent PCOS characteristic; however, it is unclear whether androgen excess, which is treatable, is a cause or a consequence of PCOS. As androgens mediate their actions via the androgen receptor (AR), we combined a mouse model of dihydrotestosterone (DHT)-induced PCOS with global and cell-specific AR-resistant (ARKO) mice to investigate the locus of androgen actions that mediate the development of the PCOS phenotype. Global loss of the AR reveals that AR signaling is required for all DHT-induced features of PCOS. Neuron-specific AR signaling was required for the development of dysfunctional ovulation, classic polycystic ovaries, reduced large antral follicle health, and several metabolic traits including obesity and dyslipidemia. In addition, ovariectomized ARKO hosts with wild-type ovary transplants displayed normal estrous cycles and corpora lutea, despite DHT treatment, implying extraovarian and not intraovarian AR actions are key loci of androgen action in generating the PCOS phenotype. These findings provide strong evidence that neuroendocrine genomic AR signaling is an important extraovarian mediator in the development of PCOS traits. Thus, targeting AR-driven mechanisms that initiate PCOS is a promising strategy for the development of novel treatments for PCOS.

PCOS | androgen | animal model | neuroendocrine

Polycystic ovary syndrome (PCOS) is the most frequent endocrine disorder of young women, with a prevalence of 6 to 15% (1), and accounts for more than 75% of anovulatory infertility (2). It is characterized by reproductive hormone dysregulation involving luteinizing hormone (LH) hypersecretion and hyperandrogenism (3), the consequences of which can be acne and hirsutism, as well as reduced fertility, due to aberrant follicular maturation, ovulatory disturbance, and miscarriage (3). Associated non-reproductive abnormalities, such as obesity, metabolic syndrome, hyperinsulinemia, insulin resistance, hepatic steatosis, and dyslipidemia predispose affected women to heightened risk of cardiovascular disease and type 2 diabetes (3, 4). However, despite the high prevalence and significant health impact, the pathogenesis of PCOS remains unclear so that mechanism-based treatments remain unattainable.

Hyperandrogenism, the most consistent feature of PCOS (5), is implicated as a key mediator in the pathogenesis of PCOS. Supportive evidence includes that androgen excess from endogenous [congenital adrenal hyperplasia (6)] or exogenous [female-to-male transsexuals (7)] sources can produce polycystic ovaries. Furthermore, androgens induce reproductive, metabolic, and endocrine features of PCOS in rodent, sheep, and primate animal models of PCOS (8–10). As all androgen action is mediated via the androgen receptor (AR), AR-mediated actions are thereby strongly implicated in the development of PCOS. Support for AR-mediated androgen actions influencing the progression of PCOS includes that variation in androgen sensitivity via the CAG triplet repeat length polymorphism of the AR (11) is associated with PCOS prevalence (12), and alternative splicing of the AR in granulosa cells is associated with aberrant follicle development (13, 14). Treatment with the AR antagonist flutamide is reported to restore ovulation in some women with PCOS (15) and rescue acyclicity (16) and anxiety-like behavior (17) in PCOS mouse models. Moreover, we recently identified that loss of AR signaling protects female mice from induction of PCOS features by prenatal hyperandrogenism (18).

Animal models have shown that systemic treatment with androgens induces PCOS-like clinical features (19); however, systemic treatments cannot elucidate the target tissue(s) of androgenic actions. Although the naming of PCOS implies a primarily ovarian condition, it has yet to be established whether the disorder originates in the ovary or elsewhere, with ovarian manifestations as downstream ramifications. We hypothesize that androgens are central in the etiology of PCOS, so in the current study we combined an optimized PCOS mouse model (20, 21) with global and neuron- and granulosa cell-specific androgen receptor knockout (ARKO) mouse lines (22, 23) to identify the sites of androgen action (Fig. 1). Our findings highlight the importance of extraovarian AR-mediated androgen actions in the origins of PCOS features, which is strongly supported by findings from recent genome-wide association studies (GWAS) of PCOS highlighting the importance of gonadotropins in PCOS (24–26).

Results

Neuron but Not Granulosa Cell AR Signaling Is Required for the Development of Anovulation in the PCOS Mouse Model. Irregular menstruation is a key diagnostic criterion for PCOS. The development

Significance

The cause of polycystic ovary syndrome (PCOS) is unknown, but androgen excess is a key feature. We combined a hyperandrogenized PCOS mouse model with global and tissue- and cell-specific androgen-resistant mouse lines to uncover the sites of androgen action that initiate PCOS. We demonstrate that direct androgen actions, particularly in neurons but less so in granulosa cells, are required for the development of key reproductive and metabolic PCOS features. These data highlight the previously overlooked importance of extraovarian neuroendocrine androgen action in the origins of PCOS. Targeting androgen-driven mechanisms may represent new options for developing a mechanism-based treatment of PCOS.

Author contributions: A.S.L.C. and K.A.W. designed research; A.S.L.C., M.C.E., R.D., M.J., and K.A.W. performed research; A.S.L.C., D.J.H., and K.A.W. analyzed data; and A.S.L.C., R.B.G., D.J.H., and K.A.W. wrote the paper.

The authors declare no conflict of interest.

This article is a PNAS Direct Submission.

See Commentary on page 4045.

[1]To whom correspondence should be addressed. Email: k.walters@unsw.edu.au.

This article contains supporting information online at www.pnas.org/lookup/suppl/doi:10.1073/pnas.1616467114/-/DCSupplemental.

www.pnas.org/cgi/doi/10.1073/pnas.1616467114

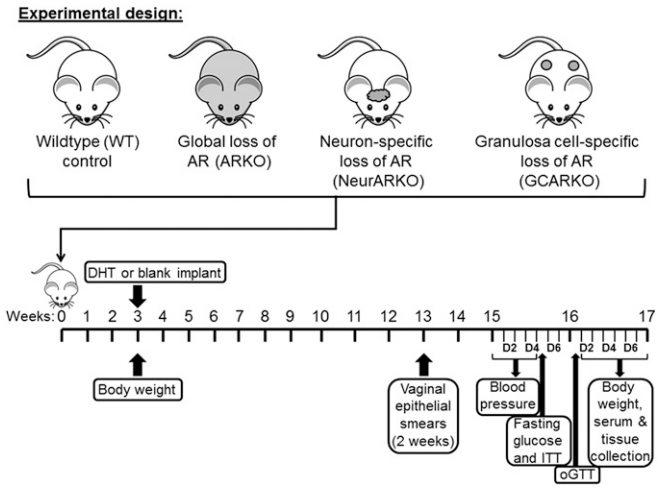

Fig. 1. Experimental design. For this study, PCOS was induced in wild-type, global, neuron-specific, and granulosa cell-specific androgen receptor knockout mice by s.c. inserting dihydrotestosterone implants in the mice for 3 mo. Control mice were implanted with blank implants. Body weight, estrous cycling, blood pressure, fasting glucose, oral glucose tolerance, and insulin tolerance were assessed before collection of serum and tissues at 16 wk of age.

of PCOS-like features in our mice was confirmed by the detection of acyclicity in 100% of WT females treated with dihydrotestosterone (DHT) ($P < 0.01$; Fig. 2*A* and Fig. S1), as well as in neuron-specific wild-type (NeurWT) (100% acyclic; $P < 0.01$) and granulosa cell-specific wild-type (GCWT) (75% acyclic; $P < 0.01$; two of the eight mice exhibiting only one long irregular cycle) females, relative to non-DHT–treated controls. In contrast, ARKO, but not NeurARKO or GCARKO (granulosa cell-specific androgen receptor knockout female mice), females maintained normal estrous-cycle patterns after DHT treatment, hence global AR inactivation protected against the development of the PCOS trait of aberrant cycles (Fig. 2*A* and Fig. S1).

Similarly, oligo/anovulation is a key reproductive characteristic of PCOS. Histologically, the number of corpora lutea (CL) present was notably diminished in DHT-treated WT, NeurWT, GCWT, and GCARKO groups, demonstrating oligo/anovulation ($P < 0.01$; Fig. 2 *B* and *C*). Conversely, global loss of AR signaling protected against the induction of ovulatory dysfunction (Fig. 2 *B* and *C*). Loss of AR signaling in granulosa cells allowed the development of DHT-induced irregular estrous cycles and ovulatory dysfunction, with GCARKO females exhibiting a significant reduction in completed estrous cycles in 2 wk ($P < 0.01$; Fig. 2*A*) and in the number of CL present in their ovaries ($P < 0.01$; Fig. 2 *B* and *C*).

NeurARKO females did not develop ovulatory dysfunction displaying multiple corpora lutea when treated with DHT (Fig. 2 *B* and *C*) but displayed apparent acyclicity according to vaginal smears (Fig. 2*A*). As androgens can directly impact vaginal epithelium (27), this apparent discrepancy of NeurARKO female cyclicity may be due to the persistence of direct DHT effects on the NeurARKO vaginal epithelium. Analysis of serum steroid levels by liquid chromatography-tandem mass spectrometry (LC-MS/MS) revealed that DHT was significantly increased in all groups of DHT-treated mice compared with strain-matched WT controls ($P < 0.01$; Table 1). DHT treatment also had significant effects on serum testosterone ($P < 0.01$) and 3α- and 3β-diol ($P < 0.01$) but not dehydroepiandrosterone (DHEA) or progesterone (P4) concentrations (Table 1). DHT treatment did not influence serum LH or follicle-stimulating hormone (FSH) levels (Table 1).

Therefore, to conclusively test the hypothesis that extraovarian AR signaling played a direct role in the development of the PCOS traits of irregular cycles and ovulatory dysfunction, we performed an independent experiment that investigated the effect of extra- and intraovarian AR signaling on these PCOS traits separately. We undertook reciprocal ovary transplants between WT and ARKO females and then induced PCOS by long-term DHT treatment. All intact WT females treated with a blank implant cycled (8 of 8), whereas 100% of intact WT females treated with DHT were acyclic (0 of 8; $P < 0.01$; Fig. 2*D*). Similarly, compared with intact control WT females with DHT treatment, 100% of WT hosts with either WT (0 of 5; $P < 0.01$) or ARKO (0 of 6; $P < 0.01$) transplanted ovaries failed to cycle, and their ovaries displayed no CL (Fig. 2 *D* and *E*). This indicates that a functional AR in the ovary is not needed for the development of aberrant cycling in PCOS. However, 71% of ARKO hosts with WT transplanted ovaries (i.e., with preserved AR signaling) cycled and their ovaries exhibited CL. This indicates that extraovarian AR actions are required for the development of the PCOS traits of aberrant estrous cycles and ovulatory dysfunction (Fig. 2 *D* and *E*). Histologically, ovaries collected from all DHT-treated WT (WT, NeurWT, or GCWT) and GCARKO females displayed the classic polycystic appearance, whereas ARKO and NeurARKO ovaries did not display that phenotype (Figs. 2*C* and 3 *C* and *D*). Ovarian weight is increased in human PCOS but decreased in this rodent PCOS model (3, 28). DHT treatment induced a significant decrease in ovary weight in all genotypes ($P < 0.01$) except for DHT-treated ARKO females, which remained comparable to control ARKO ovaries (Fig. 3*A*).

Atretic cyst-like follicles were not present in any of the control WT ovaries (WT, NeurWT, or GCWT; Figs. 2*C* and 3 *B* and *C*), but after DHT-induced PCOS all females in these groups displayed a significant increase in the prevalence of cystic follicles ($P < 0.05$; Figs. 2*C* and 3 *B–D*). Although non-DHT (blank implant)–treated ARKO females exhibited a few cystic follicles, DHT treatment to induce PCOS did not increase the numbers, consistent with global AR inactivation preventing DHT-induced cyst development. Neuron-specific loss of AR signaling significantly reduced ($P < 0.05$) but did not fully protect against the development of DHT-induced cystic follicles in NeurARKO ovaries, but was much less than that observed in DHT-treated WT and GCARKO ovaries (Figs. 2*C* and 3 *B* and *C*).

Neuron but Not Granulosa Cell AR Signaling Is Required for the Reduction in Large Antral Follicle Health in the PCOS Mouse Model. In agreement with previous studies using this PCOS mouse model (21), antral follicle populations were not altered by DHT-induced PCOS in any treated groups (Fig. S2). However, DHT treatment induced the PCOS trait of a significant increase in the proportion of morphologically unhealthy follicles in WT, NeurWT, and GCWT females, at both the small ($P < 0.01$) and large ($P < 0.05$) antral developmental stages (Fig. 4 *A* and *B*), whereas global AR insensitivity prevented the development of unhealthy antral follicles by DHT treatment of ARKO females (Fig. 4 *A* and *B*). NeurARKO ovaries displayed a protection from DHT-induced increases in unhealthy large (Fig. 4*B*) but not small ($P < 0.01$; Fig. 4*A*) antral follicles. However, a granulosa cell-specific loss of AR signaling did not protect against the DHT-induced increase in unhealthy small ($P < 0.05$) or large ($P < 0.05$) antral follicles in GCARKO ovaries (Fig. 4 *A* and *B*).

Large antral follicles in DHT-treated WT, NeurWT, and GCWT ovaries displayed a reduction in granulosa cell-layer thickness ($P < 0.01$; Fig. 4 *C* and *E*, *i* and *ii*) but a significant increase in theca cell-layer area ($P < 0.01$; Fig. 4 *D* and *E*, *iii* and *iv*). These features were fully prevented by a global loss of AR signaling (Fig. 4 *C* and *D*). Granulosa cell-specific loss of AR signaling inhibited the development of diminished granulosa cell layers but not the increase in theca cell area ($P < 0.05$; Fig. 4 *C* and *D*). Neuron-specific loss of AR signaling did not protect against DHT-induced diminished granulosa cell layers ($P < 0.05$) or an increase in theca cell-layer area ($P < 0.01$) in NeurARKO antral follicles (Fig. 4 *C* and *D*).

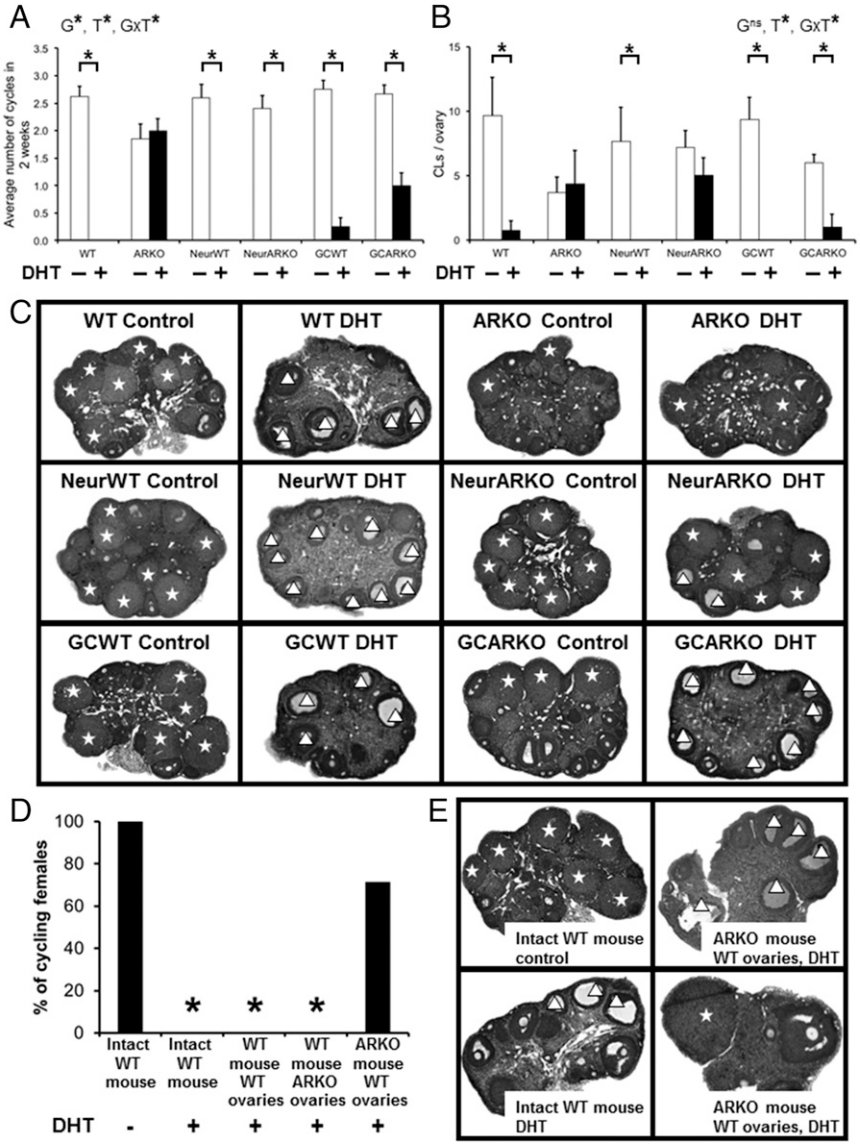

Fig. 2. Neuron but not granulosa cell AR signaling is required for the development of anovulation in the PCOS mouse model. Loss of extraovarian AR signaling ameliorates the development of acyclicity and anovulation in the PCOS mouse model. (*A*) Average number of full estrous cycles completed in a 2-wk period, confirming DHT-induced acyclicity in WT mice and showing no development of acyclicity in DHT-induced PCOS ARKO female mice. Data are the mean ± SEM; $n = 5$ to 9 per genotype/treatment group. (*B*) Average number of corpora lutea per ovary, showing no development of anovulation in DHT-induced PCOS ARKO or NeurARKO female mice. Data are the mean ± SEM; $n = 3$ to 5 per genotype/treatment group. (*C*) Histological sections of representative ovaries from each treatment group, showing the maintenance of ovulations (indicated by the presence of corpora lutea) in DHT-induced PCOS ARKO and NeurARKO ovaries. (*D*) Percentage of cycling females in a 2-wk period, showing no development of acyclicity in DHT-induced PCOS ARKO ovariectomized females transplanted with WT ovaries. (*E*) Histological sections of representative ovaries from each treatment group, showing corpora lutea in DHT-induced PCOS ARKO ovariectomized females transplanted with WT ovaries, indicative of recent ovulation. G, genotype; ns, no significant difference; T, DHT treatment; *, significant difference; star, corpora lutea; triangle, arrested antral follicle. (Magnification: 10×.) (*$P < 0.05$, two-way ANOVA.)

Neuron but Not Granulosa Cell AR Signaling Is Required for the Development of Obesity in the PCOS Mouse Model. All wild-type groups (WT, NeurWT, or GCWT) that received DHT treatment exhibited a significant increase in body weight ($P < 0.01$; Fig. 5*A*) and parametrial ($P < 0.01$; Fig. 5*B*), retroperitoneal ($P < 0.01$), inguinal ($P < 0.05$), and mesenteric fat-pad weights ($P < 0.05$). However, both global (ARKO) and neuron (NeurARKO) AR inactivation fully prevented this DHT-induced increase in body and fat-pad weights (Fig. 5). In contrast, a granulosa cell-specific loss of AR signaling did not inhibit the development of obesity, with GCARKO females displaying a significant DHT-induced increase in body weight ($P < 0.01$) and parametrial ($P < 0.01$), retroperitoneal ($P < 0.01$), inguinal ($P < 0.05$), and mesenteric ($P < 0.05$) fat-pad weights (Fig. 5 *A* and *B*).

A Loss of Neuron but Not Granulosa Cell AR Signaling Partially Protects Against the Development of Adipocyte Hypertrophy in the PCOS Mouse Model. DHT treatment induced a significant decrease in serum adiponectin levels in all DHT-treated groups ($P < 0.01$; Fig. 6*A*), except in global ARKO females, where DHT did not change serum adiponectin levels (Fig. 6*A*).

All WT groups exhibited a marked DHT-induced increase in adipocyte cell size ($P < 0.01$; Fig. 6 *B* and *C*), but this was fully prevented by global loss of AR signaling (Fig. 6 *B* and *C*). DHT treatment also resulted in adipocyte hypertrophy in NeurARKO ($P < 0.01$) and GCARKO ($P < 0.01$) mice compared with genotype-matched control mice (Fig. 6 *B* and *C*). However, the degree of adipocyte hypertrophy observed in DHT-treated

Table 1. Characterization of hormone profiles

Genotype/treatment group	DHT, ng/mL G^{ns},T^{*},GxT^{*}	T, ng/mL G^{*},T^{*},GxT^{ns}	DHEA, ng/mL G^{*},T^{ns},GxT^{ns}	3α-diol + 3β-diol, ng/mL G^{*},T^{*},GxT^{ns}	P4, ng/mL G^{ns},T^{ns},GxT^{ns}	LH, ng/mL G^{ns},T^{ns},GxT^{ns}	FSH, ng/mL G^{ns},T^{ns},GxT^{ns}
WT control	0.11 ± 0.05	0.11 ± 0.01	0.13 ± 0.02	0.24 ± 0.02	1.49 ± 0.61	0.94 ± 0.12	3.29 ± 0.38
WT DHT	0.52 ± 0.18*	0.01 ± 0.01	0.08 ± 0.02	0.09 ± 0.02	0.98 ± 0.17	0.90 ± 0.05	4.01 ± 0.58
ARKO control	0.08 ± 0.02	0.19 ± 0.08	0.11 ± 0.01	0.30 ± 0.09	0.95 ± 0.14	0.95 ± 0.23	4.80 ± 0.76
ARKO DHT	0.19 ± 0.03*	0.12 ± 0.03	0.08 ± 0.02	0.20 ± 0.04	1.18 ± 0.14	1.09 ± 0.11	3.97 ± 0.33
NeurWT control	0.06 ± 0.01	0.06 ± 0.02	0.06 ± 0.01	0.12 ± 0.02	0.99 ± 0.17	0.53 ± 0.22	3.80 ± 0.50
NeurWT DHT	0.42 ± 0.08*	0.01 ± 0.00	0.06 ± 0.01	0.07 ± 0.01	1.07 ± 0.19	0.64 ± 0.21	3.48 ± 0.47
NeurARKO control	0.05 ± 0.00	0.05 ± 0.02	0.08 ± 0.01	0.13 ± 0.03	0.84 ± 0.21	0.56 ± 0.22	2.68 ± 0.43
NeurARKO DHT	0.78 ± 0.15*	0.01 ± 0.00	0.07 ± 0.01	0.08 ± 0.01	1.45 ± 0.37	0.92 ± 0.08	3.72 ± 0.73
GCWT control	0.09 ± 0.02	0.03 ± 0.01	0.11 ± 0.03	0.14 ± 0.03	1.28 ± 0.58	0.87 ± 0.16	3.16 ± 0.51
GCWT DHT	0.57 ± 0.11*	0.01 ± 0.00	0.12 ± 0.03	0.13 ± 0.03	0.59 ± 0.16	0.75 ± 0.14	6.64 ± 1.84
GCARKO control	0.09 ± 0.02	0.07 ± 0.02	0.15 ± 0.03	0.21 ± 0.02	1.64 ± 0.79	0.95 ± 0.21	4.66 ± 0.85
GCARKO DHT	0.41 ± 0.07*	0.01 ± 0.00	0.19 ± 0.05	0.20 ± 0.05	1.94 ± 0.52	0.89 ± 0.13	3.56 ± 0.61

Serum concentrations of dihydrotestosterone, testosterone, dehydroepiandrosterone, 5α-androstane-3α,17β-diol, 5α-androstane-3β,17β-diol, progesterone, luteinizing hormone, and follicle-stimulating hormone. Data are the mean ± SEM; n = 4 to 9 per genotype/treatment group.
*Significant difference compared with strain-matched WT control female mice.

NeurARKO females was significantly less than that exhibited in all DHT-treated WT ($P < 0.01$) and GCARKO ($P < 0.01$) parametrial fat pads (Fig. 6 *B* and *C*).

Fasting glucose levels were significantly increased in all WT mice (WT, NeurWT, or GCWT) after DHT treatment ($P < 0.05$; Fig. 6*D*). Global loss of AR signaling eliminated this effect but DHT-treated NeurARKO ($P < 0.01$) and GCARKO ($P < 0.01$) mice still exhibited significantly raised fasting glucose levels (Fig. 6*D*). Similarly, an effect of DHT treatment was apparent with regard to overall glucose tolerance (two-way ANOVA main effect, $P < 0.01$; Fig. 6*E*), although DHT treatment had no effect on insulin tolerance (Fig. S3).

Neuron but Not Granulosa Cell AR Signaling Is Required for the Development of Dyslipidemia in the PCOS Mouse Model. Increased cholesterol levels were present in all DHT-treated wild-type groups ($P < 0.01$; Fig. 7*A*) but not in DHT-treated global and neuron-specific ARKO females. DHT-treated GCARKO mice still displayed the DHT-induced increase in serum cholesterol levels (Fig. 7*A*). DHT treatment had a significant effect on serum triglyceride levels (two-way ANOVA main effect, $P < 0.01$; Fig. 7*B*) with an increase in triglycerides in all three wild-type groups (WT, NeurWT, or GCWT), whereas this effect was prevented in ARKO and NeurARKO but not GCARKO female mice (Fig. 7*B*). These results suggest that DHT-induced dyslipidemia requires a functional AR in neurons but not in granulosa cells.

Systolic blood pressure was affected by DHT treatment alone (two-way ANOVA main effect, $P < 0.05$), but this effect was independent of changes in AR genotype (Fig. 7*C*).

Wild-type mice (WT, NeurWT, or GCWT) treated with DHT displayed a 10- to 20-fold increase in hepatic lipid staining compared with controls ($P < 0.01$; Fig. 7 *D* and *E*). Global loss of the AR protected against the development of DHT-induced hepatic steatosis in ARKO females. GCARKO DHT-treated mice experienced a significant increase in lipid accumulation in the liver ($P < 0.01$). Loss of neuron AR partially protected against DHT-induced hepatic steatosis, as lipid accumulation in DHT-treated NeurARKO females was significantly less than that exhibited in all DHT-treated WT ($P < 0.01$) and GCARKO ($P < 0.01$) livers (Fig. 7 *D* and *E*).

Discussion

Although hyperandrogenism is a key trait of PCOS (5) and experimentally induces a range of reproductive, endocrine, and metabolic PCOS characteristics in various animal models (8–10), the tissue- or organ-specific mechanisms through which androgens elicit these key aspects of the PCOS phenotype remain unclear. In the current study, we provide evidence that supports AR signaling as an important mediator in the development of features of experimental PCOS (Table 2). Our data demonstrate that, in particular, extraovarian neuroendocrine AR sites of androgen action are predominantly involved in the pathogenesis of multiple key PCOS characteristics. This provides strong experimental support for recent GWAS findings that highlight the importance of gonadotropin action in the genetic origins of susceptibility to PCOS (24–26). In concert, these

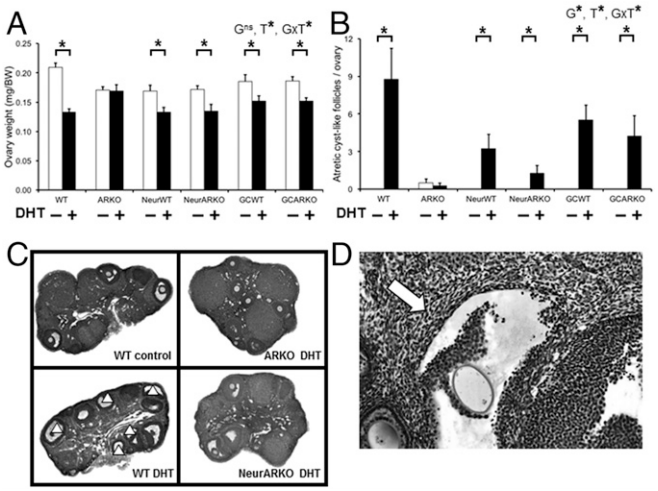

Fig. 3. Global and neuron but not granulosa cell loss of AR signaling protects against the development of the classic polycystic ovarian phenotype in the PCOS mouse model. (*A*) Ovary weights, confirming DHT-induced reduction in ovarian weight in WT mice, and showing no reduction in ovarian weight in DHT-induced PCOS ARKO female mice. Data are the mean ± SEM; n = 5 to 9 per genotype/treatment group. (*B*) Average number of atretic cyst-like follicles per ovary, displaying no significant development of cysts in DHT-induced PCOS ARKO females. Data are the mean ± SEM; n = 4 ovaries per genotype/treatment group. (*C*) Histological sections of representative ovaries, showing development of the classic PCOS ovarian phenotype in DHT-induced PCOS WT but not ARKO and NeurARKO ovaries. (*D*) Histological section of a representative cyst found in all groups treated with DHT. Cysts display a thinned and discordant granulosa cell layer, a dispersed theca cell layer (arrow), and an oocyte with a fragmented nucleolus that has lost connection with most or all of its surrounding granulosa cells. G, genotype; ns, no significant difference; T, DHT treatment; *, significant difference. (Magnification: 10×.) (*$P < 0.05$, two-way ANOVA.)

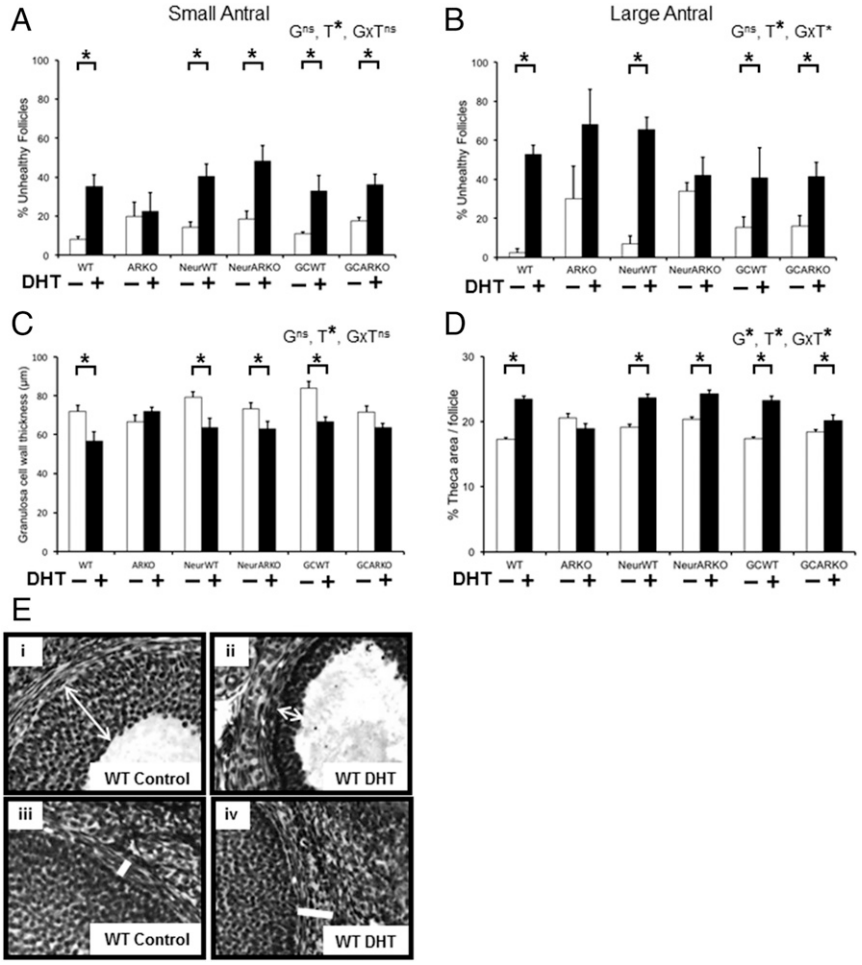

Fig. 4. Global and neuron but not granulosa cell loss of AR signaling protects against the reduction in large antral follicle health in the PCOS mouse model. (*A*) Percentage of unhealthy small antral follicles per ovary, confirming DHT-induced increase in unhealthy small antral follicles in WT mice and showing no significant decrease in small antral follicle health in DHT-induced PCOS ARKO ovaries. Data are the mean ± SEM; $n = 4$ ovaries per genotype/treatment group. (*B*) Percentage of unhealthy large antral follicles per ovary, showing no significant decrease in large antral follicle health in DHT-induced PCOS ARKO or NeurARKO female mice. Data are the mean ± SEM; $n = 4$ ovaries per genotype/treatment group. (*C*) Average thickness of granulosa cell layer per follicle, displaying no reduction in granulosa cell-layer thickness in DHT-induced PCOS ARKO or GCARKO ovaries. Data are the mean ± SEM; $n = 7$ to 24 follicles per genotype/treatment group. (*D*) Average percentage of theca area per follicle, showing no significant increase in theca cell area in DHT-induced PCOS ARKO ovaries. Data are the mean ± SEM; $n = 7$ to 24 follicles per genotype/treatment group. (*E*) Histological sections representing the effects of DHT on granulosa cell-layer thickness (*ii*, double-ended arrow) and percentage of theca area (*iv*, white line) compared with controls (*i* and *iii*, respectively). G, genotype; ns, no significant difference; T, DHT treatment; *, significant difference. (Magnification: 10×.) (*$P < 0.05$, two-way ANOVA.)

findings suggest neuroendocrine AR signaling as a key target for the development of novel mechanism-based PCOS treatments.

Our data show, by combining a DHT-induced PCOS mouse model with global and tissue- and cell-specific ARKO mouse models, that the induction of the PCOS traits of acyclicity and anovulation requires AR signaling. These findings are in agreement with clinical evidence supporting a direct role for androgen actions in the development of dysfunctional menstrual cycling and ovulation in PCOS, as prolonged treatment with the AR antagonist flutamide is reported to restore menstrual-cycle regularity and ovulation in some women with PCOS (15, 29). Interestingly, by contrast, the treatment of women with PCOS with estrogen blockage, either by antiestrogen (clomiphene citrate) or an aromatase inhibitor (letrozole) that increases FSH secretion, is rapidly effective at inducing ovulation (30). This implies that the hypothalamic–pituitary feedback response in PCOS women is functional but that the longer time to effective treatment by androgen blockade may involve more complex, possibly multistep underlying mechanisms of androgen-mediated effects, compared with the more direct mode of action of estrogen blockade. Importantly, our findings highlight the importance of extraovarian AR actions in the pathogenesis of ovulatory dysfunction in PCOS. We show that females treated with DHT display aberrant ovulatory function when they have fully functional AR actions (intact WT females and ovariectomized WT females bearing WT ovary transplants) or a loss of AR signaling in the ovary only (GCARKO females and ovariectomized WT females bearing ARKO ovary transplants). However, females with an extraovarian loss of AR actions (NeurARKO females and ovariectomized ARKO females bearing WT ovary transplants) are protected against DHT-induced reduction in ovulation, indicated by reduced numbers of corpora lutea. This suggests that hyperandrogenism-induced PCOS requires AR actions in neurons and that the AR in granulosa cells is less involved in the development of PCOS acyclicity. There was a discrepancy between the ovulatory function and cyclicity in NeurARKO and a lack of an overall significant effect on serum P4 and LH, most likely due to all cycling mice being collected on the afternoon of diestrus, when serum P4 and LH levels are very low. Nevertheless, the presence of corpora lutea in NeurARKO ovaries conclusively confirms the occurrence of recent ovulations. In addition, by undertaking

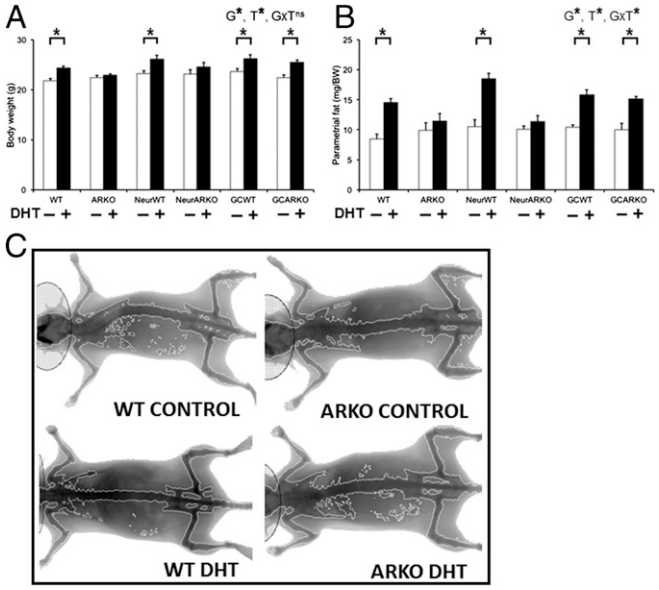

Fig. 5. Global and neuron but not granulosa cell loss of AR signaling protects against the development of obesity in the PCOS mouse model. (*A*) Body weight, confirming DHT-induced increased body weight in WT mice and showing no significant increase in body weight in DHT-induced PCOS ARKO or NeurARKO female mice. Data are the mean ± SEM; $n = 5$ to 9 mice per genotype/treatment group. (*B*) Parametrial fat deposit weight, showing no significant increase in adiposity in DHT-induced PCOS ARKO or NeurARKO female mice. Data are the mean ± SEM; $n = 5$ to 9 per genotype/treatment group. (*C*) Representative dual-energy X-ray absorptiometry images, showing no development of obesity in DHT-induced PCOS ARKO female mice. G, genotype; ns, no significant difference; T, DHT treatment; *, significant difference. (*$P < 0.05$, two-way ANOVA.)

reciprocal ovary transplants between WT and ARKO females, we decisively proved that extraovarian AR signaling is crucial in the development of the PCOS traits of irregular cycles and ovulatory dysfunction. Taken together with the recent GWAS findings that implicate alterations in gonadotropin secretion in the origins of PCOS (24–26), our findings support the previous hypothesis that hyperandrogenism may impair neuronal circuits in the brain, leading to a disruption in sex steroid feedback mechanisms and abnormal gonadotrophin secretion, and subsequent ovulatory dysfunction (31, 32). Current evidence from a mouse PCOS model points to a role for androgen excess in promoting impaired progesterone-sensitive gamma-aminobutyric acid (GABA)ergic input to GnRH neurons within the arcuate nucleus of the hypothalamus (32). Although species differences occur between humans and rodents in the site of action of positive estradiol feedback required to trigger the ovulatory LH surge (33), it is clear that alterations in GnRH pulse generation are present in women with PCOS (34).

Classic PCOS multicystic ovaries were observed in all DHT-treated WT groups, whereas this was prevented by global and neuronal loss of AR actions, confirming that AR-mediated androgen action is required for the development of this key feature of PCOS. Similarly, the PCOS ovarian morphological features of reduced follicular health and antral follicle granulosa cell-layer attenuation but theca cell-layer hypertrophy were induced by DHT in all WT mice but were not present in DHT-treated ARKO females. Furthermore, large antral follicle health was maintained in DHT-treated NeurARKO ovaries, whereas granulosa cell-wall thickness was not attenuated in GCARKO females. This finding, together with the observation that a few DHT-treated GCARKO females display intermittent cycles and some corpora lutea, implies that in addition to extraovarian androgen action, additional loci of ovarian AR actions are involved in mediating the PCOS reproductive phenotype.

Obesity is very common among women with PCOS and in turn leads to more severe hyperandrogenism (5, 35). We observed significant increases in body and fat-pad weights in all DHT-treated WT females, whereas global and neuron-specific disruption of AR signaling protected females from increased adiposity, implying that hyperandrogenism is directly involved in the high prevalence of obesity in women with PCOS. Supportive clinical evidence comes from findings that obese PCOS women consuming a hypocaloric diet together with an androgen antagonist (flutamide) exhibited additional favorable decreases in visceral fat compared with diet alone (36, 37).

Adipocyte dysfunction is also linked to PCOS pathogenesis (38, 39). Adiponectin, postulated to be a beneficial adipokine due to its insulin-sensitizing property and antiatherogenic action (40), is reduced in women with PCOS (41). Treatment with adiponectin in a rat model of PCOS ameliorates the PCOS phenotype by reversing acyclicity and PCOS ovarian features, and also improves glucose homeostasis (42). Serum adiponectin levels were reduced in our PCOS mouse model, and this effect was protected by global loss of AR function but not by neuron- or granulosa cell-specific loss of AR actions. Altered adipose structure has been reported in PCOS women (43) and is linked with androgen excess, as prenatally androgenized female monkeys display impaired adipogenesis (44). Adipocyte hypertrophy and hepatic steatosis (resembling nonalcoholic fatty liver disease) were exhibited in all DHT-treated wild-type groups but absent in global ARKO females. Granulosa cell-specific loss of AR signaling did not protect against these lipid metabolic PCOS traits, but a neuron-specific loss of AR actions did offer partial protection, implying that other sites of AR signaling are required for full development of these traits. Although hypertrophic adipocytes are inherently insulin-resistant, insulin resistance was not present in any of the DHT-treated mice. Nevertheless, glucose homeostasis was consistently impaired, with elevated fasting glucose levels observed in all DHT-treated wild-type groups as well as neuron- and granulosa cell-specific ARKO females, whereas global AR loss prevented the fasting hyperglycemic effects of DHT treatment. Altered glucose homeostasis in conjunction with the increase in hepatic steatosis observed in DHT-treated wild-type groups indicates a significant role for AR signaling in regulating glycogenolysis. Dyslipidemia, a key risk factor for cardiovascular disease, was observed in all DHT-treated wild-type females. Global or neuron-specific loss of AR signaling prevented DHT-induced dyslipidemia, as opposed to mice lacking granulosa cell AR, which developed the condition. Further studies are needed to understand how central AR signaling in particular leads to the lipid metabolic disturbance of PCOS. However, the findings that increased s.c. fat mass and cholesterol levels induced by a high-fat diet can be alleviated in ovariectomized female mice treated with DHT (45) indicate that a balance in direct AR actions is required to maintain normal metabolic function.

By combining unique global and cell-specific ARKO mouse models with a PCOS mouse model, we have revealed that hyperandrogenism, acting directly via the AR and independent of estrogenic effects, is required for the development of several key PCOS traits in an experimental mouse model. None of the inducible features of PCOS observed in WT mice were generated in mice with a global AR inactivation, indicating that AR-mediated androgen actions are critical in the pathogenesis of these traits. Our present findings extend our previous findings that global androgen insensitivity prevents the induction of experimental PCOS features in mature mice (18). Moreover, we provide evidence to support a hypothesis that the development of many key PCOS traits does not require AR signaling in granulosa cells but rather that anovulation, impaired antral follicle health, obesity, and lipid metabolic disturbance are all dependent

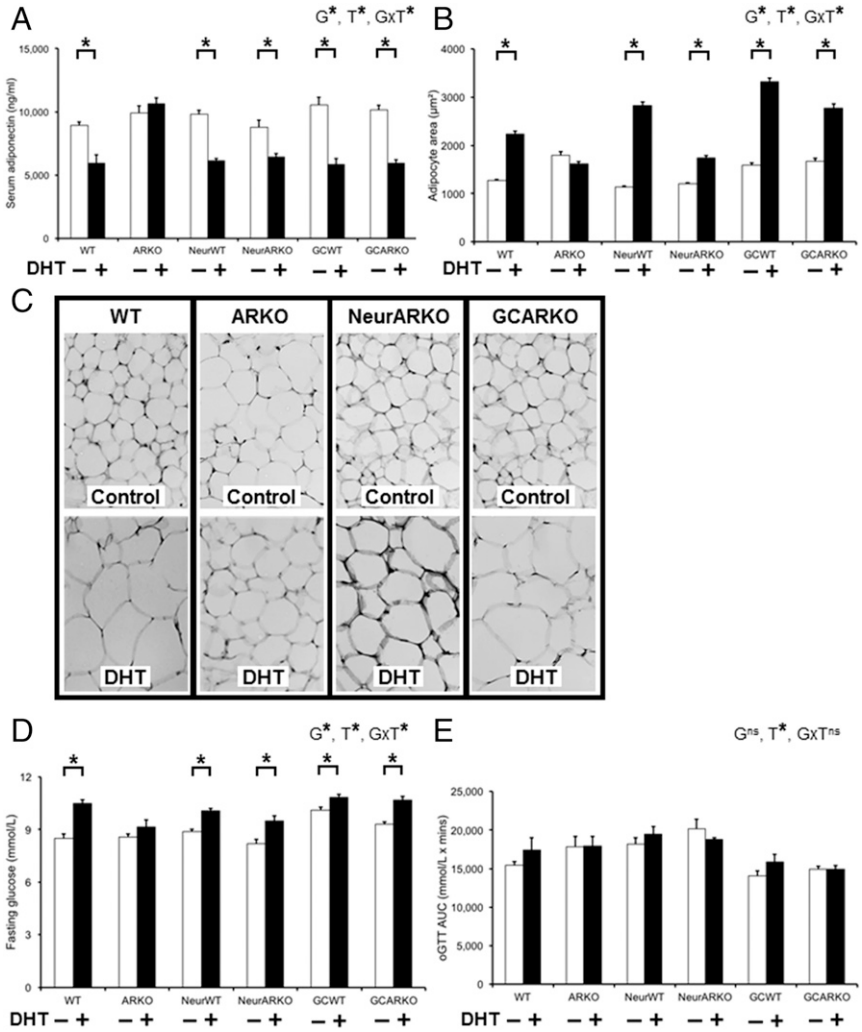

Fig. 6. Global loss of AR signaling protects against the reduction in adiponectin levels, adipocyte hypertrophy, and altered glucose homeostasis in the PCOS mouse model. (*A*) Serum levels of adiponectin, confirming DHT-induced suppression of serum adiponectin levels in WT mice and showing no significant reduction in adiponectin levels in DHT-induced PCOS ARKO female mice. Data are the mean ± SEM; $n = 5$ to 7 per genotype/treatment group. (*B*) Adipocyte size, showing no development of adipocyte hypertrophy in DHT-induced PCOS ARKO female mice. Data are the mean ± SEM; $n = 3$ sections per mouse, 3 mice per genotype/treatment group. (*C*) Histological sections of representative parametrial fat pads from each treatment group, showing no development of adipocyte hypertrophy in DHT-induced PCOS ARKO female mice. (*D*) Average fasting glucose levels showing no significant increase in glucose levels in DHT-induced PCOS ARKO female mice. Data are the mean ± SEM; $n = 5$ to 9 per genotype/treatment group. (*E*) Area under the curve (AUC) analysis of the oral glucose tolerance test, showing an overall effect of DHT treatment. Data are the mean ± SEM; $n = 5$ to 9 per genotype/treatment group. G, genotype; ns, no significant difference; T, DHT treatment; *, significant difference. (Magnification: 40×.) (*$P < 0.05$, two-way ANOVA.)

on a functional neuronal AR signaling network. However, neither NeurARKO nor GCARKO mouse models fully protected against the development of all PCOS traits. This indicates that the development of some PCOS pathology requires direct AR-mediated androgen actions acting via other sites, or are a downstream response to the altered PCOS environment. These findings demonstrate the complexity of the mechanisms regulating PCOS pathogenesis, and support the notion that the development of PCOS involves hyperandrogenic actions acting within multiple tissues. Taken together, our findings provide strong evidence that hyperandrogenism plays a direct pathogenic role involving a neuroendocrine site of action in the development of key PCOS traits, and support a more tissue- and/or AR-mediated targeted approach in the development of novel therapeutic treatments.

Materials and Methods

Mice. Mice were maintained under standard housing conditions (ad libitum access to food and water in a temperature- and humidity-controlled, 12-h light/dark environment) at the ANZAC Research Institute. All surgical procedures were carried out under ketamine/xylazine anesthesia, whereas nonsurgical procedures were carried out under an isoflurane inhalation anesthetic. All procedures were approved by the Sydney Local Health District Animal Welfare Committee within National Health and Medical Research Council guidelines for animal experimentation.

Experimental Design. To elucidate the site of AR-mediated androgen actions in the etiology of PCOS, three mouse lines with site-specific loss of AR signaling were examined: (*i*) androgen receptor knockout mice with global loss of AR signaling; (*ii*) neuron-specific ARKO mice with brain-specific loss of AR signaling; and (*iii*) granulosa cell-specific ARKO mice lacking granulosa cell AR signaling. Each were compared with their relevant wild-type controls. All six groups were treated without (controls) or with long-term exposure to dihydrotestosterone postnatally (Fig. 1), which induces PCOS in wild-type mice as previously described (21) and based on prior reports of DHT induction of experimental PCOS in rats (28) and mice (20). Briefly, 3-wk-old female mice were implanted with either a 1-cm Silastic implant (i.d., 1.47 mm; o.d., 1.95 mm; Dow Corning; 508-006) containing about 10 mg DHT or an empty, blank control. All DHT-treated experimental groups exhibited a

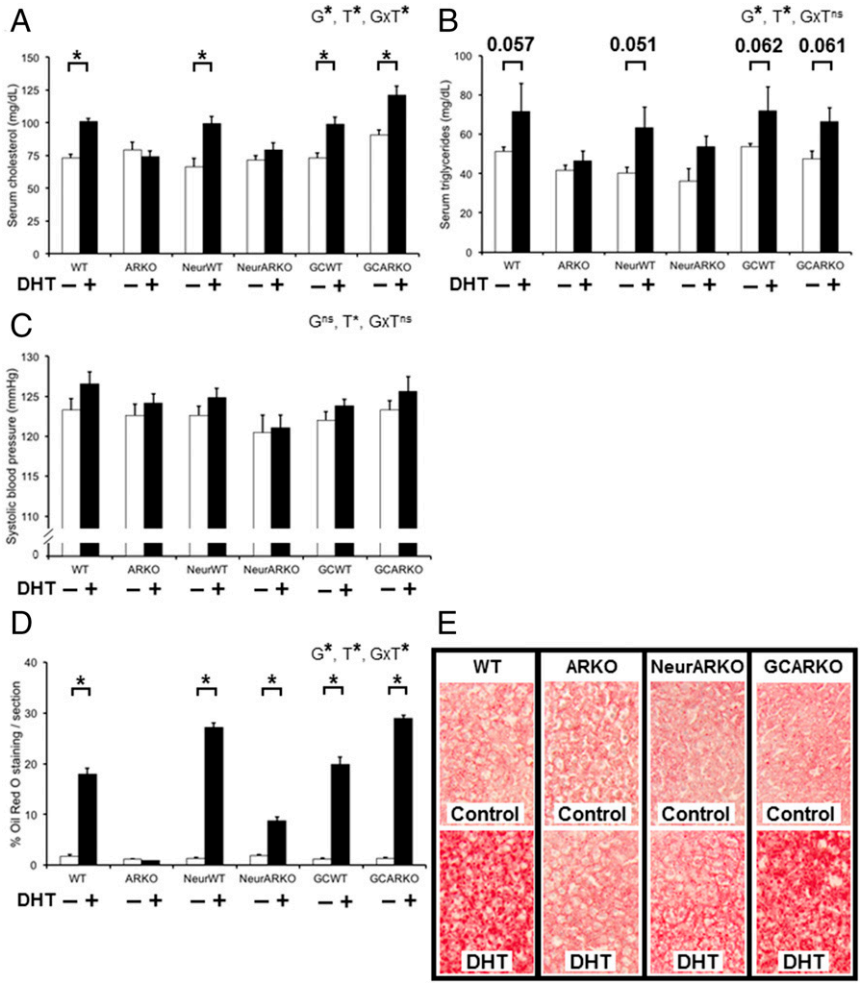

Fig. 7. Global and neuron but not granulosa cell loss of AR signaling ameliorates the development of dyslipidemia in the PCOS mouse model. (*A*) Serum cholesterol levels, confirming DHT-induced increased serum cholesterol in WT mice and showing no significant increase in cholesterol levels in DHT-induced PCOS ARKO or NeurARKO female mice. Data are the mean ± SEM; $n = 5$ to 7 per genotype/treatment group. (*B*) Serum triglyceride levels, showing an overall effect of DHT treatment and a nonsignificant trend to increased triglyceride levels in all DHT-treated groups, apart from DHT-induced PCOS ARKO and NeurARKO female mice. Data are the mean ± SEM; $n = 5$ to 7 per genotype/treatment group. (*C*) Systolic blood pressure, displaying no significant difference between control and DHT-treated PCOS mice of any genotype. Data are the mean ± SEM; $n = 5$ to 9 per genotype/treatment group. (*D*) Analysis of liver steatosis by oil red O staining, showing no significant increase in the presence of steatosis in DHT-induced PCOS ARKO female mice. Data are the mean ± SEM; $n = 3$ sections per mouse, 3 mice per genotype/treatment group. (*D*) Histological sections of representative liver sections stained with oil red O, showing reduced lipid staining in DHT-induced PCOS ARKO livers. G, genotype; ns, no significant difference; T, DHT treatment; *, significant difference. (Magnification: 40×.) (*$P < 0.05$, two-way ANOVA.)

significant increase in serum DHT levels (Table 1; $P < 0.01$). Mice were collected after ∼13 wk of drug administration (WT: control $n = 7$, DHT $n = 8$; ARKO: control $n = 7$, DHT $n = 7$; NeurWT: control $n = 5$, DHT $n = 5$; NeurARKO: control $n = 5$, DHT $n = 5$; GCWT: control $n = 8$, DHT $n = 8$; GCARKO: control $n = 9$, DHT $n = 9$), when the mice were ∼16 wk of age.

Generation and Genotyping of ARKO, GCARKO, and NeurARKO Mice. Homozygous female ARKO mice were generated by crossing ARflox mice (46), in which exon 3 is flanked by loxP sites, with Sox2-Cre mice (47) as a universal deletor, as previously described (48). Female GCARKO mice were generated by crossing ARflox mice (46) with AMH-Cre mice (49), as previously reported (23). To generate female NeurARKO mice, ARflox mice (46) were mated with transgenic CamKIIα-Cre mice (50). Genomic DNA isolated from toe clip or tail biopsy was used as a template for PCR genotyping to detect rearrangements in the mouse *Ar* gene, as described (22). Mice containing the Sox2-Cre gene or the AMH-Cre gene were detected using primers and PCR conditions as described (23, 48). Mice containing the CamKIIα-Cre gene were detected using the following PCR primers: Cre1: 5′-GGTTCTCCGTTTGCACTC-3′; Cre2: 5′-CTGCATGCACGGGACAGCTCT-3′; and Cre3: 5′-GCTTGCAGGTACAGGAGGTA-3′. Two products are obtained in Cre-positive mice: 375 bp for transgenic Cre and 290 bp for endogenous Cre. All knockout models were confirmed using RT-PCR for appropriate, tissue-specific inactivation of the AR using RNA extracted from ovary, uterus, brain, and pituitary (Fig. S4), as described (22). Primers specific for mouse β-actin were used as an internal control. Baseline phenotypic characteristics of the different ARKO mouse models are provided in Table S1.

Ovarian Transplantation. Reciprocal paired ovarian transplants were performed between wild-type and ARKO females as well as between wild-type and wild-type females as surgical controls for the procedure, as previously described (51). Females served as both donors and recipients whenever possible. Four-week-old mice were anesthetized, and each ovary was exposed via a flank incision. The surrounding bursa was incised and the ovary was gently removed at the hilum. After excision from the donor, the ovaries were held in cold sterile saline until placed inside the ovarian bursa of the ovariectomized recipient. A single stitch of 8-0 silk suture was placed through the incision in the bursa. The reproductive tract was then returned to its normal anatomical position and the abdominal wall and skin were closed using 6-0 silk sutures. At the same time as mice underwent ovarian transplantation, females were also implanted with a DHT implant or blank implant as described above.

Assessment of Estrous Cycle. Estrous-cycle stage was analyzed using vaginal epithelial cell smears taken daily for 14 consecutive days (21). Smears were

Table 2. Summary of the effect of global, neuron-specific, and granulosa cell-specific loss of androgen receptor signaling on the development of PCOS traits

		+ DHT		
Clinical PCOS trait	WT mouse	Global loss of AR	Neuronal loss of AR	Granulosa cell loss of AR
Absent/irregular cycling	✓	✗	✓	Partial
Oligo/anovulation	✓	✗	✗	✓
Classic multicystic ovarian appearance	✓	✗	Partial	✓
Change in ovary weight*	✓	✗	✓	✓
↑Unhealthy small antral follicles	✓	✗	✓	✓
↑Unhealthy large antral follicles	✓	✗	✗	✓
↓Granulosa cell-layer thickness	✓	✗	✓	✗
↑Theca cell-layer thickness	✓	✗	✓	✓
↑Body weight	✓	✗	✗	✓
↑Parametrial fat-pad weight	✓	✗	✗	✓
↑Retroperitoneal fat-pad weight	✓	✗	✗	✓
↑Inguinal fat-pad weight	✓	✗	✗	✓
↑Mesenteric fat-pad weight	✓	✗	✗	✓
Adipocyte hypertrophy	✓	✗	Partial	✓
↓Adiponectin	✓	✗	✓	✓
Dyslipidemia†	✓	✗	✗	✓
Hepatic steatosis	✓	✗	Partial	✓
Impaired fasting glucose	✓	✗	✓	✓

✓, clinical PCOS trait present; ✗, clinical PCOS trait not present; partial, effect of DHT evident but not to the same extent seen in WT mice.

*↑ In humans; ↓ in mice.

†↑Cholesterol + clear trend toward ↑triglycerides.

collected at the same time each day (10 AM) using 15 μL of 0.9% sterile saline, transferred to glass slides to air dry. Dry smears were stained with 0.5% toluidine blue before being examined under a light microscope. Estrous-cycle stage was determined based on the presence or absence of leukocytes, cornified epithelial cells, and nucleated epithelial cells. Proestrus was characterized by the presence of mostly nucleated and some cornified epithelial cells; at the estrus stage, primarily cornified epithelial cells were present; at metestrus, both cornified epithelial cells and leukocytes were present; and at diestrus, predominantly leukocytes were present.

Ovary Preparation, Morphological Analysis, and Follicle Health. Dissected ovaries were weighed, fixed in 4% (volvol) paraformaldehyde overnight at 4 °C, and stored in 70% ethanol before histological processing. Ovaries were processed through graded alcohols and embedded in glycol methacrylate resin (Technovit 7100; Heraeus Kulzer). Serial sections of 20 μm were stained with periodic acid-Schiff and counterstained with hematoxylin. For CL quantification, whole-section scans of every second section were taken under a light microscope using the EVOS FL Auto System (Life Technologies). To quantify antral follicle populations and assess follicular health, sections were examined using an Olympus light microscope with Stereo Investigator software (MBF Bioscience), as previously described (21). Total numbers of small antral follicles (oocyte surrounded by greater than five layers of granulosa cells and/or one or two small areas of follicular fluid), large antral follicles (containing a single large antrum), preovulatory follicles (a large antral follicle with an oocyte surrounded by cumulus cells at the end of a stalk of mural granulosa cells), and atretic cyst-like follicles (large fluid-filled cysts with an attenuated granulosa cell layer, dispersed theca cell layer, and an oocyte lacking connection to the granulosa cells; Fig. 3*D*) were classified and quantified as previously reported (21, 22). To avoid repetitive counting, each follicle was only counted in the section where the oocyte's nucleolus was visible. For all analyses, large antral follicles and preovulatory follicles were grouped together and called "large antral follicles." Follicles were classified as unhealthy if they contained a degenerate oocyte and/or more than 10% of the granulosa cells were pyknotic in appearance, as previously described (21, 22). The proportion of unhealthy follicles per ovary was calculated as the percentage of all follicles at that developmental stage. For all large antral follicles, granulosa cell-layer thickness and theca cell-layer area were measured using ImageJ version 1.48 software (open-source, developed by the National Institutes of Health), as previously reported (21).

Hormone Assays. Blood was collected from females by cardiac exsanguination under ketamine/xylazine anesthesia, and collected serum was stored at −20 °C. Mouse serum LH and FSH were determined using a species-specific immunofluorometric assay, as previously described (18). The mouse LH detection limit was 0.04 ng/mL, intraassay coefficient of variation (CV) was 5.2%, and interassay CV was 8.6%. The mouse FSH detection limit was 0.1 ng/mL, intraassay CV was 3.1%, and interassay CV was 7.2%. All immunoassays were performed in a single batch.

Serum levels of testosterone (T), DHEA, DHT, its two principal metabolites 5α-androstane-3α,17β-diol (3α-diol) and 5α-androstane-3β,17β-diol (3β-diol), and progesterone were measured in extracts of 100 μL mouse serum by LC-MS/MS, as previously described (18). The limits of quantitation (defined as the lowest level that can be detected with a CV of <20%) were 25 pg/mL for T, 100 pg/mL for DHEA, DHT, 3α-diol, and 3β-diol, and 50 pg/mL for P4.

Adipose Tissue Analysis. Parametrial fat pads were weighed, fixed in 4% paraformaldehyde, embedded in paraffin, and sectioned at 8 μm. Sections were stained with hematoxylin and eosin before images were taken for histomorphometry at 40× magnification under a light microscope using the EVOS FL Auto System (Life Technologies). Five distinct images were taken from each of three sections of the fat pad, with at least 200 μm separating these sections.

Hepatic Steatosis Analysis. Livers were weighed whole before the right lateral lobe was excised from the whole liver and fixed in 10% neutral buffered formalin overnight at 4 °C and then soaked in 30% sucrose (vol/vol) for 48 h; 1-cm × 1-cm segments were excised from the lobe and embedded in OCT compound (Tissue-Tek) before 10-μm sections were cryosectioned and air-dried onto slides. Slides were stained with oil red O in 60% isopropanol to visualize lipid deposition, as previously described (52), before histomorphometric analysis. ImageJ version 1.48 software (NIH) was used to quantify oil red O-positive staining. Three separate images were analyzed from three distinct sections taken at least 200 μm apart.

Insulin and Oral Glucose Tolerance Tests. Insulin tolerance tests (ITTs) and oral glucose tolerance tests (oGTTs) were carried out as previously reported, with modifications (52). Mice were fasted for 6 h before a baseline blood glucose reading, followed by an i.p. injection of 0.75 IU/kg body weight (BW) insulin (Eli Lilly) or an oral bolus of glucose at 2 g/kg BW. Blood glucose was then measured at 15, 30, 60, 90, and 120 min. Blood was obtained from a tail prick, and blood glucose was measured on glucose strips and an Accu-Chek glucometer (Roche). ITTs and oGTTs were carried out at 16 wk of age.

Blood Pressure. Blood pressure was measured with an automated tail-cuff system (MC4000; Hatteras Instruments), as previously described (53). Animals were acclimatized to the system for 3 d before data being collected on the fourth day. Animals were conscious at the time of measurement. Measurements were taken at 16 wk of age.

Cholesterol and Triglyceride Assays. Serum levels of triglycerides and total cholesterol were assayed enzymatically with kits obtained from Wako (Cholesterol E Kit, 439-17501; Triglyceride Kit, 432-40201).

Adiponectin Assay. Serum levels of total full-length mouse adiponectin were measured using a Quantikine ELISA Kit from R&D Systems (MRP300) according to the manufacturer's instructions. The mean minimum detectable dose of mouse adiponectin was 0.003 ng/mL. This kit specifically measures natural and recombinant full-length mouse adiponectin; <0.5% cross-reactivity is observed with available related molecules.

Statistical Analysis. Statistical analysis was performed using Prism 6 software (GraphPad Software). Data that were not normally distributed were transformed before analysis using log transformation. Statistical differences were tested by two-way ANOVA followed by Fisher's least significant difference multiple-comparison test as a post hoc test. Proportions were analyzed by Fisher's exact test. P values <0.05 were considered statistically significant.

ACKNOWLEDGMENTS. We thank Professor Brian Oldfield (Monash University) for access to the CamKIIα-Cre mice, Jenny Spaliviero for technical support, and Dr. Blake Cochran (University of New South Wales) for his thoughtful and helpful discussions. This work was supported by a National Health and Medical Research Council project grant (APP1022648).

1. Fauser BC, et al. (2012) Consensus on women's health aspects of polycystic ovary syndrome (PCOS): The Amsterdam ESHRE/ASRM-Sponsored 3rd PCOS Consensus Workshop Group. *Fertil Steril* 97(1):28–38.e25.
2. Gorry A, White DM, Franks S (2006) Infertility in polycystic ovary syndrome: Focus on low-dose gonadotropin treatment. *Endocrine* 30(1):27–33.
3. Dumesic DA, et al. (2015) Scientific statement on the diagnostic criteria, epidemiology, pathophysiology, and molecular genetics of polycystic ovary syndrome. *Endocr Rev* 36(5):487–525.
4. Shorakae S, Boyle J, Teede H (2014) Polycystic ovary syndrome: A common hormonal condition with major metabolic sequelae that physicians should know about. *Intern Med J* 44(8):720–726.
5. Nisenblat V, Norman RJ (2009) Androgens and polycystic ovary syndrome. *Curr Opin Endocrinol Diabetes Obes* 16(3):224–231.
6. Pignatelli D (2013) Non-classic adrenal hyperplasia due to the deficiency of 21-hydroxylase and its relation to polycystic ovarian syndrome. *Front Horm Res* 40:158–170.
7. Pache TD, Fauser BC (1993) Polycystic ovaries in female-to-male transsexuals. *Clin Endocrinol (Oxf)* 39(6):702–703.
8. Walters KA, Allan CM, Handelsman DJ (2012) Rodent models for human polycystic ovary syndrome. *Biol Reprod* 86(5):149.
9. Padmanabhan V, Veiga-Lopez A (2013) Sheep models of polycystic ovary syndrome phenotype. *Mol Cell Endocrinol* 373(1–2):8–20.
10. Abbott DH, et al. (2013) Nonhuman primate models of polycystic ovary syndrome. *Mol Cell Endocrinol* 373(1–2):21–28.
11. Simanainen U, et al. (2011) Length of the human androgen receptor glutamine tract determines androgen sensitivity in vivo. *Mol Cell Endocrinol* 342(1–2):81–86.
12. Baculescu N (2013) The role of androgen receptor activity mediated by the CAG repeat polymorphism in the pathogenesis of PCOS. *J Med Life* 6(1):18–25.
13. Wang F, et al. (2015) Alternative splicing of the androgen receptor in polycystic ovary syndrome. *Proc Natl Acad Sci USA* 112(15):4743–4748.
14. Walters KA, Handelsman DJ (2016) Androgen receptor splice variants and polycystic ovary syndrome: Cause or effect? *Asian J Androl* 18(3):442–443.
15. Rittmaster RS (1999) Antiandrogen treatment of polycystic ovary syndrome. *Endocrinol Metab Clin North Am* 28(2):409–421.
16. Sullivan SD, Moenter SM (2004) Prenatal androgens alter GABAergic drive to gonadotropin-releasing hormone neurons: Implications for a common fertility disorder. *Proc Natl Acad Sci USA* 101(18):7129–7134.
17. Hu M, et al. (2015) Maternal testosterone exposure increases anxiety-like behavior and impacts the limbic system in the offspring. *Proc Natl Acad Sci USA* 112(46):14348–14353.
18. Caldwell AS, et al. (2015) Haplosufficient genomic androgen receptor signaling is adequate to protect female mice from induction of polycystic ovary syndrome features by prenatal hyperandrogenization. *Endocrinology* 156(4):1441–1452.
19. Walters KA (2015) Role of androgens in normal and pathological ovarian function. *Reproduction* 149(4):R193–R218.
20. van Houten EL, et al. (2012) Reproductive and metabolic phenotype of a mouse model of PCOS. *Endocrinology* 153(6):2861–2869.
21. Caldwell AS, et al. (2014) Characterization of reproductive, metabolic, and endocrine features of polycystic ovary syndrome in female hyperandrogenic mouse models. *Endocrinology* 155(8):3146–3159.
22. Walters KA, et al. (2007) Female mice haploinsufficient for an inactivated androgen receptor (AR) exhibit age-dependent defects that resemble the AR null phenotype of dysfunctional late follicle development, ovulation, and fertility. *Endocrinology* 148(8):3674–3684.
23. Walters KA, et al. (2012) Targeted loss of androgen receptor signaling in murine granulosa cells of preantral and antral follicles causes female subfertility. *Biol Reprod* 87(6):151.
24. Tian Y, et al. (2016) Variants in FSHB are associated with polycystic ovary syndrome and luteinizing hormone level in Han Chinese women. *J Clin Endocrinol Metab* 101(5):2178–2184.
25. Day FR, et al. (2015) Causal mechanisms and balancing selection inferred from genetic associations with polycystic ovary syndrome. *Nat Commun* 6:8464.
26. Hayes MG, et al.; Reproductive Medicine Network (2015) Genome-wide association of polycystic ovary syndrome implicates alterations in gonadotropin secretion in European ancestry populations. *Nat Commun* 6:7502.
27. Kimura T, Basu SL, Nandi S (1967) Nature of induced persistent vaginal cornification in mice. 3. Effects of estradiol and testosterone on vaginal epithelium in vitro. *J Exp Zool* 165(3):497–503.
28. Mannerås L, et al. (2007) A new rat model exhibiting both ovarian and metabolic characteristics of polycystic ovary syndrome. *Endocrinology* 148(8):3781–3791.
29. Paradisi R, Fabbri R, Battaglia C, Venturoli S (2013) Ovulatory effects of flutamide in the polycystic ovary syndrome. *Gynecol Endocrinol* 29(4):391–395.
30. Kar S (2012) Clomiphene citrate or letrozole as first-line ovulation induction drug in infertile PCOS women: A prospective randomized trial. *J Hum Reprod Sci* 5(3):262–265.
31. Blank SK, McCartney CR, Helm KD, Marshall JC (2007) Neuroendocrine effects of androgens in adult polycystic ovary syndrome and female puberty. *Semin Reprod Med* 25(5):352–359.
32. Moore AM, Prescott M, Marshall CJ, Yip SH, Campbell RE (2015) Enhancement of a robust arcuate GABAergic input to gonadotropin-releasing hormone neurons in a model of polycystic ovarian syndrome. *Proc Natl Acad Sci USA* 112(2):596–601.
33. Plant TM (2012) A comparison of the neuroendocrine mechanisms underlying the initiation of the preovulatory LH surge in the human, Old World monkey and rodent. *Front Neuroendocrinol* 33(2):160–168.
34. Taylor AE, et al. (1997) Determinants of abnormal gonadotropin secretion in clinically defined women with polycystic ovary syndrome. *J Clin Endocrinol Metab* 82(7):2248–2256.
35. Moran LJ, Norman RJ, Teede HJ (2015) Metabolic risk in PCOS: Phenotype and adiposity impact. *Trends Endocrinol Metab* 26(3):136–143.
36. Gambineri A, et al. (2003) Anti-androgen treatment increases circulating ghrelin levels in obese women with polycystic ovary syndrome. *J Endocrinol Invest* 26(7):629–634.
37. Gambineri A, et al. (2004) Effect of flutamide and metformin administered alone or in combination in dieting obese women with polycystic ovary syndrome. *Clin Endocrinol (Oxf)* 60(2):241–249.
38. Barber TM, Franks S (2013) Adipocyte biology in polycystic ovary syndrome. *Mol Cell Endocrinol* 373(1–2):68–76.
39. Chen X, Jia X, Qiao J, Guan Y, Kang J (2013) Adipokines in reproductive function: A link between obesity and polycystic ovary syndrome. *J Mol Endocrinol* 50(2):R21–R37.
40. Chakraborti CK (2015) Role of adiponectin and some other factors linking type 2 diabetes mellitus and obesity. *World J Diabetes* 6(15):1296–1308.
41. Mannerås-Holm L, et al. (2011) Adipose tissue has aberrant morphology and function in PCOS: Enlarged adipocytes and low serum adiponectin, but not circulating sex steroids, are strongly associated with insulin resistance. *J Clin Endocrinol Metab* 96(2):E304–E311.
42. Yuan X, et al. (2016) Brown adipose tissue transplantation ameliorates polycystic ovary syndrome. *Proc Natl Acad Sci USA* 113(10):2708–2713.
43. Dumesic DA, et al. (2016) Hyperandrogenism accompanies increased intra-abdominal fat storage in normal weight polycystic ovary syndrome women. *J Clin Endocrinol Metab* 101(11):4178–4188.
44. Keller E, et al. (2014) Impaired preadipocyte differentiation into adipocytes in subcutaneous abdominal adipose of PCOS-like female rhesus monkeys. *Endocrinology* 155(7):2696–2703.
45. Fagman JB, et al. (2015) The androgen receptor confers protection against diet-induced atherosclerosis, obesity, and dyslipidemia in female mice. *FASEB J* 29(4):1540–1550.
46. Notini AJ, Davey RA, McManus JF, Bate KL, Zajac JD (2005) Genomic actions of the androgen receptor are required for normal male sexual differentiation in a mouse model. *J Mol Endocrinol* 35(3):547–555.
47. Hayashi S, Lewis P, Pevny L, McMahon AP (2002) Efficient gene modulation in mouse epiblast using a Sox2Cre transgenic mouse strain. *Mech Dev* 119(Suppl 1):S97–S101.
48. Cheng XB, et al. (2013) Characterizing the neuroendocrine and ovarian defects of androgen receptor-knockout female mice. *Am J Physiol Endocrinol Metab* 305(6):E717–E726.
49. Lécureuil C, Fontaine I, Crepieux P, Guillou F (2002) Sertoli and granulosa cell-specific Cre recombinase activity in transgenic mice. *Genesis* 33(3):114–118.
50. Casanova E, et al. (2001) A CamKIIalpha iCre BAC allows brain-specific gene inactivation. *Genesis* 31(1):37–42.
51. Walters KA, et al. (2009) Subfertile female androgen receptor knockout mice exhibit defects in neuroendocrine signaling, intraovarian function, and uterine development but not uterine function. *Endocrinology* 150(7):3274–3282.
52. Brennan-Speranza TC, et al. (2012) Osteoblasts mediate the adverse effects of glucocorticoids on fuel metabolism. *J Clin Invest* 122(11):4172–4189.
53. Solon-Biet SM, et al. (2014) The ratio of macronutrients, not caloric intake, dictates cardiometabolic health, aging, and longevity in ad libitum-fed mice. *Cell Metab* 19(3):418–430.